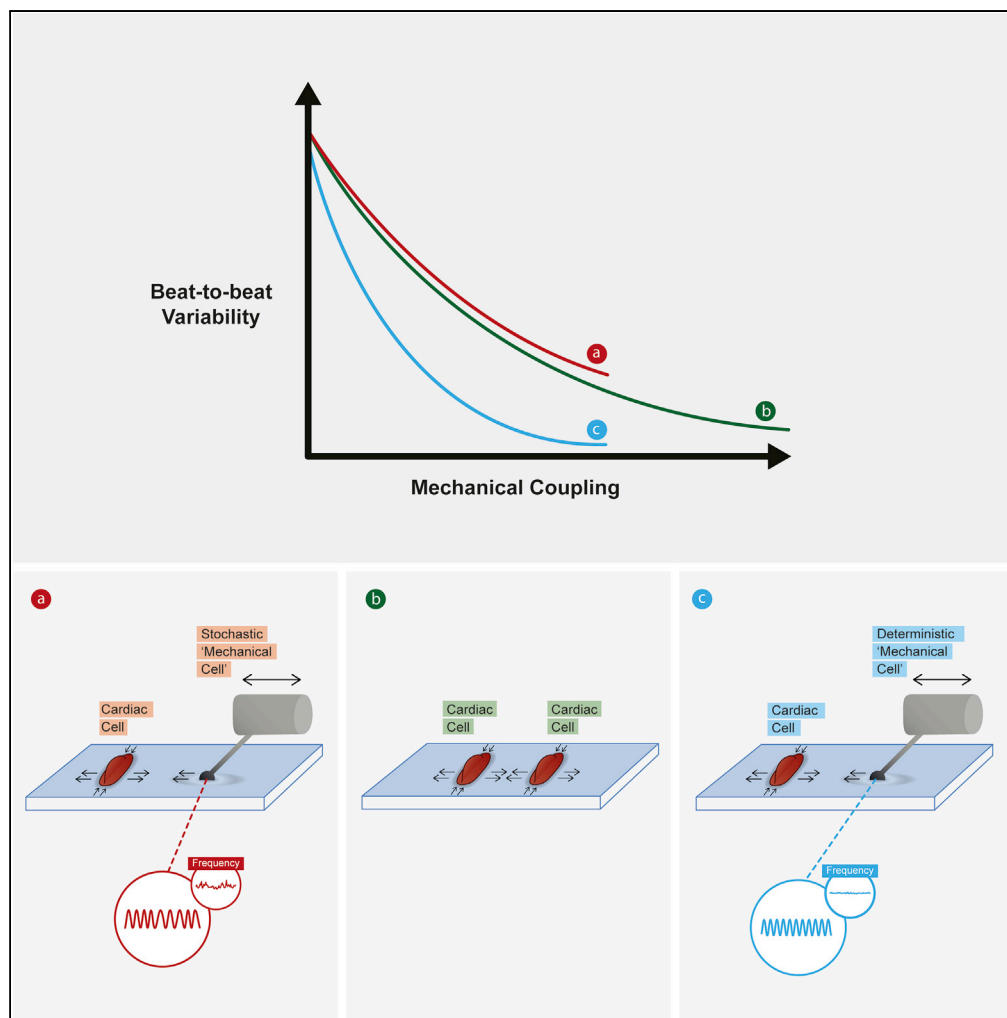


Article

Mechanical Communication Acts as a Noise Filter



Hen Viner, Ido Nitsan, Liel Sapir, Stavit Drori, Shelly Tzliil

shellytz@technion.ac.il

HIGHLIGHTS

Mechanical communication reduces intrinsic noise in interacting cells

Cardiac cell beating noise decays exponentially with the strength of mechanical coupling

Identical exponential decay length is obtained using a stochastic mechanical cell

NOX2, ROS, and CaMKII are involved in mechanical communication-induced noise reduction

Viner et al., iScience 14, 58–68
April 26, 2019 © 2019 The Author(s).
<https://doi.org/10.1016/j.isci.2019.02.030>

Article

Mechanical Communication Acts as a Noise Filter

Hen Viner,^{1,2} Ido Nitsan,^{1,2} Liel Sapir,¹ Stavit Drori,¹ and Shelly Tzliil^{1,3,*}

SUMMARY

Cells can communicate mechanically by responding to mechanical deformations generated by their neighbors. Here, we describe a new role for mechanical communication by demonstrating that mechanical coupling between cells acts as a signaling cue that reduces intrinsic noise in the interacting cells. We measure mechanical interaction between beating cardiac cells cultured on a patterned flexible substrate and find that beat-to-beat variability decays exponentially with coupling strength. To demonstrate that such noise reduction is indeed a direct consequence of mechanical coupling, we reproduce the exponential decay in an assay where a beating cell interacts mechanically with an artificial stochastic ‘mechanical cell’. The mechanical cell consists of a probe that mimics the deformations generated by a stochastically beating neighboring cardiac cell. We show that noise reduction through mechanical coupling persists long after stimulation stops and identify microtubule integrity, NOX2, and CaMKII as mediators of noise reduction.

INTRODUCTION

It was recently established that cells are able to communicate mechanically by responding to mechanical deformations generated by their neighbors (Nitsan et al., 2016; Viner et al., 2009; Tang et al., 2011; Angelini et al., 2010; Chiou et al., 2016; Cohen and Safran, 2016; Reinhart-King et al., 2008). Exploring matrix-mediated mechanical cell-cell communication is experimentally challenging since it is difficult to isolate this specific contribution from all other modes of communication, such as electrical and chemical. However, several instances of mechanical communication through the matrix were demonstrated unequivocally. These include collective cell migration (Reinhart-King et al., 2008; Angelini et al., 2010), cell alignment (Viner et al., 2009; Engler et al., 2004), and cardiac cell beating (Nitsan et al., 2016; Chiou et al., 2016). Nevertheless, the characteristics of mechanical communication and its range, role, and ability to regulate biochemical processes within the cell are still largely unknown (Sapir and Tzliil, 2017). Cellular processes, such as protein synthesis, post-translational modification, or trafficking, undergo stochastic fluctuations—“noise”—in their levels and activities. Here we show that mechanical coupling acts as a noise filter that reduces the intrinsic noise of interacting cells.

Spontaneous beating of cardiac cells arises from self-sustained oscillations of the intercellular calcium concentration coupled to membrane depolarization-repolarization cycles (Quinn and Kohl, 2012; Maltsev and Lakatta, 2009). The beating rate is regulated by the kinetics and sensitivity of ion channels (e.g., L-type Ca^{2+} channel) and transporters (e.g., $\text{Na}^+/\text{Ca}^{2+}$ exchanger) at the plasma membrane and by calcium pumps and release channels (e.g., Ryanodine receptors [RyRs]) in the sarcoplasmic reticulum (Yang et al., 2002; Lakatta et al., 2010). Channel phosphorylation by cellular enzymes, such as protein kinase A and Ca^{2+} /calmodulin-dependent protein kinase II (CaMKII), affects channel kinetics and sensitivity. The stochastic nature of these biochemical reactions and of channel opening events makes the spontaneous beating of a single cardiac cell stochastic as well (Heijman et al., 2013), with intrinsic noise manifested as variability in the time between consecutive contractions (beat-to-beat variability). Isolated spontaneously beating cardiac cells have large beat-to-beat variability that must be reduced to allow for synchronized contraction.

We have previously shown that spontaneously beating cardiac cells can be paced using a ‘mechanical cell’, which consists of a tungsten probe that mimics the deformations generated by a neighboring beating cardiac cell (Nitsan et al., 2016). There was no physical contact between the cell and the probe, and the interaction therefore was purely mechanical and mediated through propagation of deformations in the underlying substrate. However, the mechanical cell generated deterministic oscillatory deformations and cardiac cell beating is stochastic. The stochastic nature of cardiac cell beating raises

¹Faculty of Mechanical Engineering, Technion – Israel Institute of Technology, Haifa 32000, Israel

²These authors contributed equally

³Lead Contact

*Correspondence:

shellytz@technion.ac.il

<https://doi.org/10.1016/j.isci.2019.02.030>



several questions such as: Is beating stochasticity regulated by mechanical coupling? Can a stochastically beating cell mechanically pace its neighbor and reduce its intrinsic noise?

Here, we directly measure mechanical interaction between isolated pairs of cardiac cells cultured on a flexible substrate that enables mechanical coupling through propagation of mechanical deformations in the substrate, with no physical contact between the cells. We find that beat-to-beat variability decreases exponentially with coupling strength. To corroborate that decreased beating variability is indeed a direct consequence of mechanical coupling, we reproduce the exponential decay in an assay in which a beating cell interacts mechanically with a 'mechanical cell'. By turning the probe into a stochastic 'mechanical cell', the exponential decay constant converged to that obtained for pairs of mechanically coupled living cardiac cells.

Mechanical communication cannot be regarded as a simple displacement but as a signaling cue that transmits information through a cascade of biochemical reactions. Recent theoretical work demonstrated that a signaling network can function as a filter that suppresses noise (Hinczewski and Thirumalai, 2014). We show that the propagation of the mechanical signal through the cellular signaling network does exactly that. We use a stochastic 'mechanical cell' to pace an isolated beating cell and reduce its beat-to-beat variability. Beating variability is reduced below the noise of the stochastic 'mechanical cell', and both pacing and noise reduction persist after stimulation stops, consistent with long-term modifications that occur within the cardiac cell that affect its intrinsic stochasticity. By quantitatively measuring the reduction of noise with mechanical coupling strength in the presence of different inhibitors, we could identify microtubule integrity, NOX2 (nicotinamide adenine dinucleotide phosphate-oxidase 2), and CaMKII as mediators of mechano-chemo-transduction in this case.

RESULTS

Mechanical Coupling between Cells Reduces Beat-to-Beat Variability

Primary neonatal rat cardiac cells were cultured on either matrigel-coated or laminin-coated polyacrylamide gels with an elastic modulus of 3.8 ± 0.2 kPa as measured by atomic force microscopy. Substrate stiffness in this range was shown to support optimal spontaneous cardiac cell beating for neonatal cardiac cells in culture (Engler et al., 2008; Nitsan et al., 2016; Majkut et al., 2013). Part of the experiments were repeated with a slightly softer gel (1 ± 0.15 kPa). By incorporating 0.2- μ m fluorescent beads in the polyacrylamide substrate and tracking their movement over time, we could quantify the deformation field generated by a beating cardiac cell and extract its beating signal (see Videos S1 and S2 and Figure S2). As demonstrated previously, a pair of aligned beating cells, with no physical contact between them, which reside at a distance that allows their deformation fields to overlap, synchronize their spontaneous average beating frequency (Nitsan et al., 2016). However, although the pair is synchronized in their average frequency, they go in and out of phase as a result of their beat-to-beat variability (see, for example, Figure 1 and Video S1). To study the dependence of beat-to-beat variability on the strength of mechanical coupling, we cultured cells on patterned substrates (Transparent Methods and Figure 2A). Using the patterned substrate, the dimensions of the cardiac cells and the distance between neighboring cells and their relative orientation were controlled.

Spontaneously beating cardiac cells vary in their contractile amplitude, and generally, cells within a pair beat with different contraction amplitudes. In the extreme case, one of the cells contracts with an amplitude large enough to induce significant strain next to its neighbor, whereas its neighbor generates deformations that are much smaller and do not propagate all the way to the first cell. We regard this case as a 'master'/ 'slave' behavior since only one of the cells generates strain field large enough to influence its neighbor. Surprisingly, in cases that are close to this scenario, the 'master' appears to contract with high beat-to-beat variability, whereas the 'slave' beats steadily with extremely low beat-to-beat variability (Figure 1 and Videos S1 and S2). Although it seems counter intuitive at first, the high variability of the 'master' cell is consistent with the high beat-to-beat variability of an isolated spontaneous beating cardiac cell in culture (Figure S1). This suggests that the slave follows the average beating frequency of the 'master' (Figures 1A and 1B), whereas its beat-to-beat variability is reduced as a consequence of the strong coupling to its neighbor (Figure 1). The 'master', on the other hand, can barely detect the strain generated by its neighbor and can therefore be thought of as a nearly isolated beating cardiac cell in culture.

This master/slave phenomenon is a limiting behavior, and in most pairs of cells, there are no clear master and slave. Nevertheless, within all pairs of cardiac cells observed ($n = 30$, see Figure 2), the cell that senses

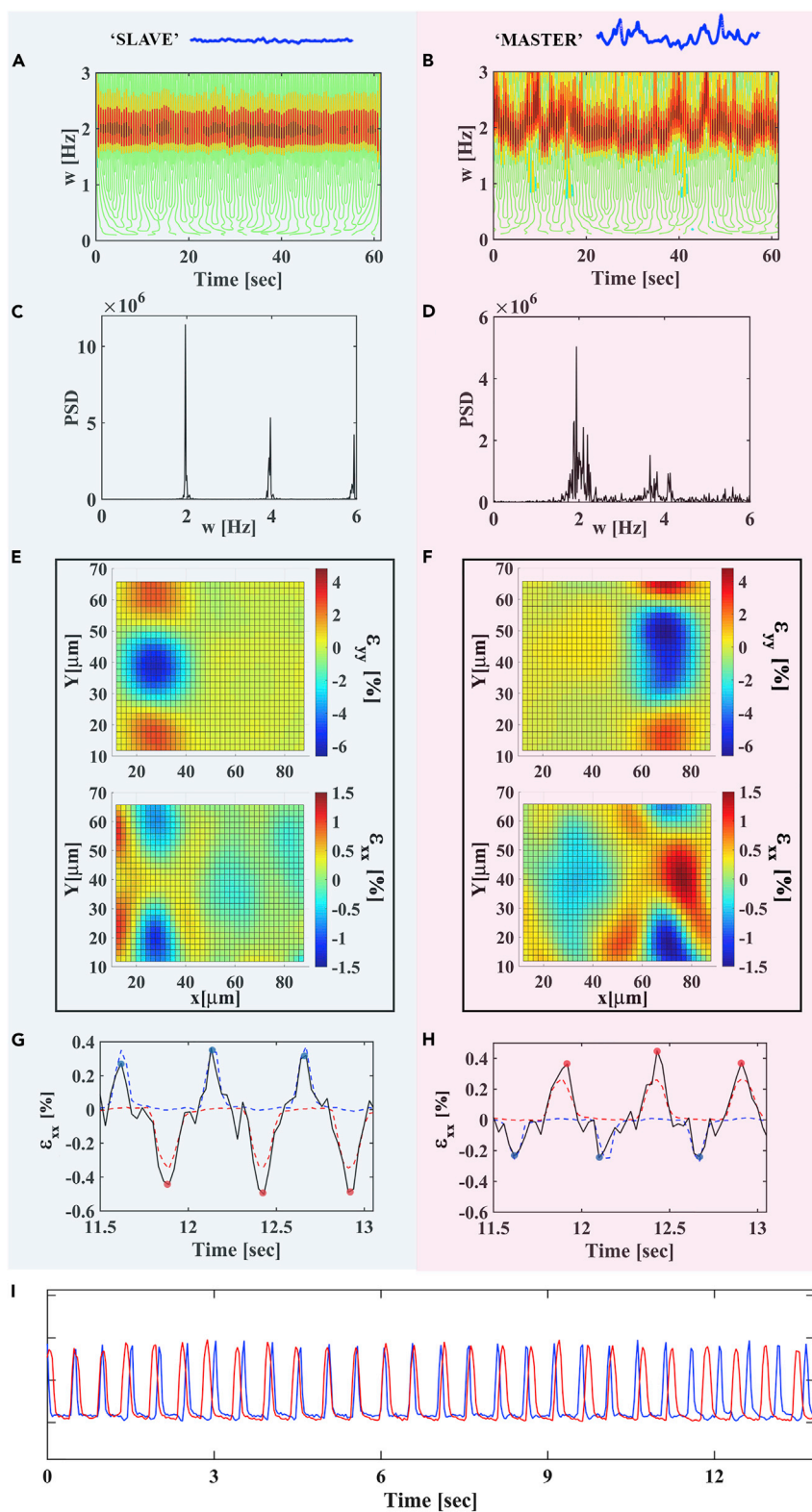


Figure 1. Mechanical Coupling Reduces Beating Variability

A representative pair of spontaneously beating cardiac cells 20 μm apart on a flexible substrate. The average frequency is synchronized; however, the right cell is highly stochastic and weakly coupled to the left cell, while the left cell, which is

Figure 1. Continued

strongly coupled mechanically to the right cell, beats steadily with low variability. This suggests that the left cell ('slave') follows the average beating frequency of the right cell ('master'), whereas its beat-to-beat variability is reduced as a consequence of the strong coupling to the right cell. The left panel (A, C, E, and G) corresponds to the left cell, whereas the right panel (B, D, F, and H) describes the behavior of the right cell. (A) and (B) show the transient frequency vs. time calculated using wavelet analysis; (C) and (D) are the corresponding Fourier transforms (power spectral density [PSD]). (E) and (F) are the strain field generated by the beating cells along the contraction axis (y axis, top) and along the vector connecting to two cells (x axis, bottom). The strain field is shown for a time point where the neighboring cell is relaxed. (G and H), The black curve shows the average strain at the edge of the beating cell along the x axis. The blue and red curves are the normalized beating signals of the left and right cells, respectively, for a short time period where the cells beat in anti-phase (part of the signal shown in I) and are only shown to mark the time position of cell contraction. When the cells beat in anti-phase, we can differentiate between the strain generated by the cell itself and by its neighbor. The strain peaks marked with red dots result from contractions of the right cell, whereas the strain peaks marked with blue dots result from contractions of the left cell. Mechanical coupling for the left cell is calculated as $\chi_L = |\epsilon_{xx,R}(x=L)/\epsilon_{xx,L}(x=L)|$, i.e., by dividing the average strain values generated by the right cell at the edge of the left cell (red dots) by the average strain generated by the left cell next to its edge (blue dots). (I), The blue and red curves are the normalized beating signals of the left and right cells, respectively, for a short time period. Videos showing the fluorescent beads in the underlying substrate (where contractions are apparent) and the calculated strain maps for this time period can be found in the [Supplemental Information \(Videos S1 and S2\)](#).

the deformations generated by its neighbor the most has lower beat-to-beat variability, whereas its neighbor beats more stochastically.

Noise Is Reduced Exponentially with Mechanical Coupling to a Neighboring Cell

To systematically explore the phenomenon described earlier and study the quantitative dependence of beat-to-beat variability on the strength of mechanical coupling, we define a mechanical coupling parameter that describes the level of mechanical coupling between a cardiac cell and its neighbor. Cells sense the deformation field at their edge, which is the sum of the deformations they generate and the ones generated by neighboring beating cells. The neighboring cell is expected to have a significant influence when its deformations are on the same order of magnitude or higher, as the ones generated by the cell itself. We therefore define mechanical coupling as the ratio between the deformations generated by a neighboring cell at the cell edge and those generated by the cell itself. This ratio defines how strong the perturbation generated by the neighboring cell is. More formally, we define a mechanical coupling parameter χ , such that $\chi = |\epsilon_{xx,n}/\epsilon_{xx,c}|$, where $\epsilon_{xx,n}$ is the strain generated by the neighboring cell along the vector connecting the two cells (x axis) and $\epsilon_{xx,c}$ is the strain generated by the cell itself (Figures 1G, 1H, S2, and S3).

The beating noise (beat-to-beat variability) ξ was calculated as the relative standard deviation (SD) of the beating frequency, $\xi = \sigma_\omega / \langle \omega \rangle$, where $\langle \omega \rangle$ is the average beating frequency of the cell and σ_ω is the SD. An alternative definition that gave very similar results is the relative SD of the time between consecutive contractions, $\xi_{\Delta t} = \sigma_{\Delta t} / \langle \Delta t \rangle$. Typical beating profiles and beating noise values for spontaneous beating cardiac cells in culture are shown in [Figure S1](#).

As shown in [Figure 2B](#), the beating noise (ξ) decays exponentially with the strength of mechanical coupling (χ) according to $\xi = ae^{-k\chi}$, where k is the exponential decay constant. The inverse value of the decay constant is the value of mechanical coupling required for the noise to decay by a factor of $1/e$. As such, when the decay constant is larger, the effect of mechanical communication on noise is stronger, the exponent decays faster, and a lower value of mechanical coupling is required to achieve noise reduction. The decay constant of the beating noise with the strength of mechanical coupling to a beating neighboring cell is 2.43 ± 0.19 ([Figure 2B](#)) ($n = 30$ cells). The same result holds when the noise is estimated using $\xi_{\Delta t}$ with a decay constant of 2.2 ± 0.14 ($n = 30$ cells, [Figure 2D](#)). Mechanical coupling is determined by the deformations generated by the neighboring cells ([Figure 2C](#)). These deformations are a function of substrate stiffness, the distance between cells and beating amplitude. Since we directly measure the strain field and use it to calculate the strength of mechanical coupling, we can combine data from cells within different distances, cultured on different substrate rigidities and coatings ([Figures 2 and S4](#)). Spontaneously beating cardiac cells in culture differ in their beat-to-beat variability ([Figure S1](#)) and might in principle have different sensitivities to mechanical coupling. It is therefore not trivial that cells that belong to different pairs still fall on the same exponential curve. This result indicates that noise reduction by mechanical coupling is highly robust.

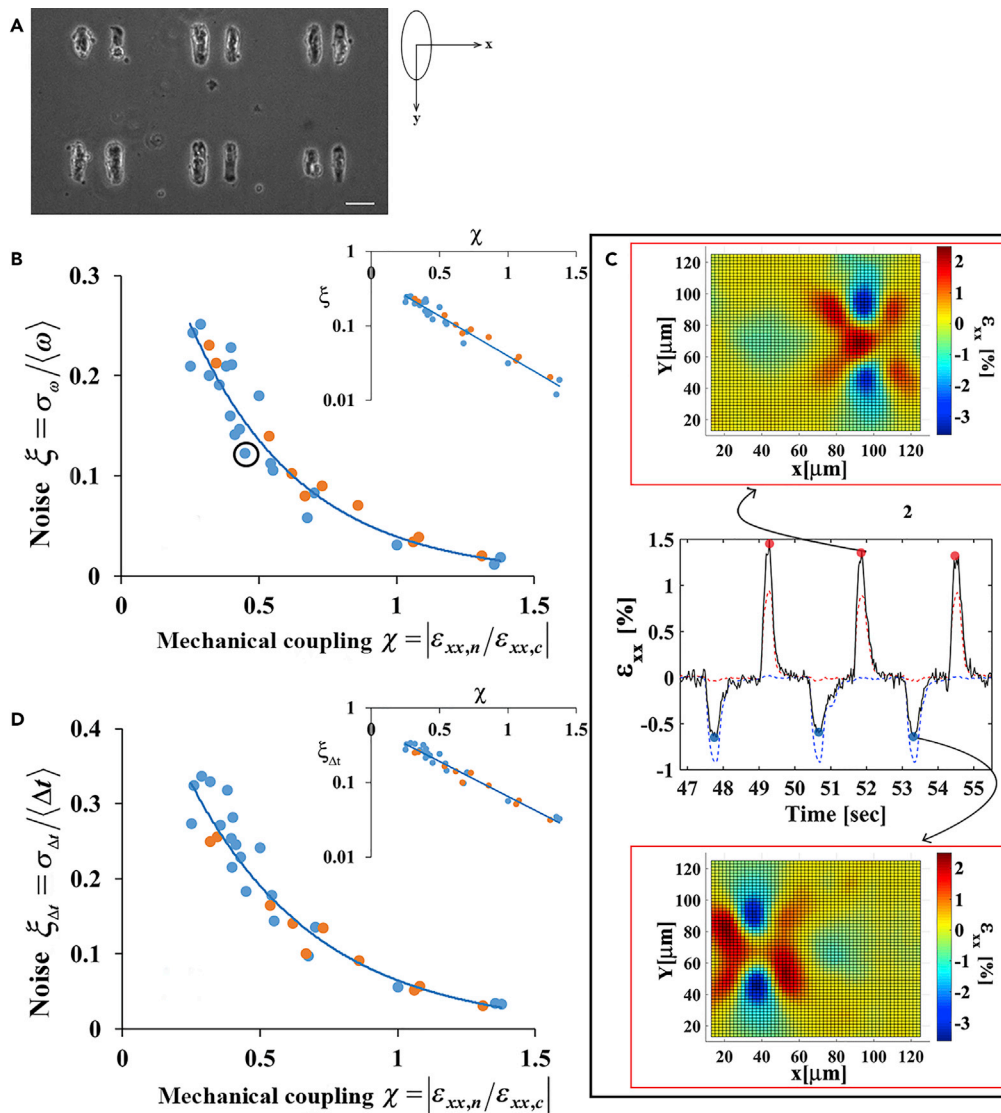


Figure 2. Noise Is Reduced Exponentially with Mechanical Coupling

(A) A representative image of isolated pairs of cardiac cells on a pattern. Notice that there is no physical contact between the cells. Scale bar is: 50 μm . We use an axis system whereby the cells are aligned along the y axis. Using this coordination system, the contraction axis of the cell (the long axis) is the y axis and the x axis is the direction of the vector connecting the two cells. A beating cardiac cell generates deformations on a flexible substrate in the x-direction, in addition to the ones in the y-direction owing to the Poisson's effect.

(B and D) Beating noise decays exponentially with the strength of mechanical coupling to a neighboring cell. Beating noise, defined as the relative SD of the beating frequency (B) or as the relative SD of the time between consecutive beatings (D), is plotted as a function of mechanical coupling. The insets in (B) and (D) show the noise in a logarithmic scale. The decay constant in (B) and (D) is 2.43 ± 0.19 and 2.2 ± 0.14 , respectively. SDs were calculated using the bootstrap method. The predictive power of the model was assessed using leave-one-out cross-validation. For both (B) and (D): the blue and orange circles represent cells that were cultured on 4 kPa and 1 kPa substrates, respectively. $n = 30$ cells are shown from 8 different cultures and 16 different dishes. R^2 values for A and B are reported in Table S1 in the Supplemental Information.

(C) Demonstration of the calculation of mechanical coupling for a representative pair of beating cardiac cells (the point marked in [B]), for additional details see Figure S2). In short, the black curve shows the average strain at the edge of the beating cell in the x-direction. The blue and red curves are the normalized beating signals of the left and right cells, respectively, for a short time period in which the cells beat in anti-phase and are only shown to mark the time position of cell contraction. The strain peaks marked with red dots result from contractions of the right cell, whereas the strain peaks marked with blue dots result from contractions of the left cell. Therefore, mechanical coupling for the right cell is

Figure 2. Continued

calculated as $\chi_R = |\epsilon_{xx,L}(x = R) / \epsilon_{xx,R}(x = R)|$, i.e., by dividing the average strain values generated by the left cell at the edge of the right cell (blue dots) by the average strain generated by the right cell next to its edge (red dots). Since the strain generated by the right cell next to its edge is positive, whereas the strain generated by its neighbor is negative, we use the absolute value of this ratio. Strain maps at two time points are shown.

Noise Is Reduced Exponentially with Mechanical Coupling to a ‘Mechanical Cell’

To ensure that the reduction of noise is indeed a direct consequence of mechanical coupling and does not result from indirect effects, such as a change in the amount or type of secreted chemo-attractants, we used a ‘mechanical cell’ (also referred to as a mechanical probe) as previously described (Nitsan et al., 2016). In short, we replaced one of the cells with a mechanical device that consists of a tungsten probe mounted on a piezo-stage. The mechanical probe deforms the substrate such as to mimic the mechanical deformations generated by a beating cardiac cell. There is no physical contact between the cell and the probe, and the interaction therefore is solely mechanical and mediated through propagation of deformations in the underlying substrate. Figure 3A illustrates schematically the experimental setup. The mechanical interaction with the ‘mechanical cell’ was quantified in the same way it was done for two neighboring beating cells, i.e., by calculating the ratio between the strain generated at the cell edge by the probe and the strain generated by the cell itself (Figure 3B). Probe frequency was set equal to the average frequency of the beating cardiac cell to separate the effect of pacing a cardiac cell from that of noise reduction. By gradually increasing the amplitude of probe oscillations, the beating noise of the cardiac cell could be monitored as a function of the strength of mechanical interaction with the probe for the same cell. We let the cell interact with the probe for 10 minutes before recording the signal and changing the amplitude. This was done to allow the cell to reach stationary behavior. For each cell, beat-to-beat variability was found to decay exponentially with the strength of mechanical coupling (Figure 3C). Although filtering noise may affect the mean of the original signal (Rackauckas et al., 2018), the frequency of the cell and its beating amplitude did not change for different values of mechanical coupling; only the noise was reduced (Figure S5).

The exponential decays obtained for different cells all converged to the same exponential curve after normalizing with respect to the beating variability of the isolated cell before probe activation (with a decay constant of 5.5 ± 0.23 , Figure 3D). This is consistent with the behavior observed for pairs of mechanically coupled cardiac cells. Again, these results demonstrate the robustness of the phenomenon of noise reduction through mechanical coupling.

Pacing and Noise Reduction of a Cardiac Cell Using a Stochastic ‘Mechanical Cell’

Interestingly, beating noise decays more rapidly with mechanical coupling when a cell interacts with a ‘mechanical cell’ compared with the decay obtained for an interaction with a living cardiac cell (Figure 3D, $p < 0.0004$ using linear mixed effects model with random slope). A clear difference between these assays is that the mechanical probe is deterministic, whereas the living cell is stochastic. To explore the influence of the stochastic nature of spontaneous beating on mechanical communication, we turned our mechanical probe into a stochastic mechanical cell. We did so by generating frequencies of oscillations from a Gaussian distribution with a SD comparable to the beating variability observed in isolated beating cardiac cells (Figures S1 and 4A).

We monitored beating noise as a function of the strength of mechanical interaction with the stochastic probe while gradually increasing the probe average amplitude. Here again, the exponential decays obtained for different cells all converged to the same exponential curve after normalizing with respect to the beating variability of the isolated cell before probe activation (with a decay constant of 2.4 ± 0.11 , Figure 3D). However, now, taking the cardiac cell beating stochasticity into account, it is converged to the exponential decay obtained for pairs of mechanically coupled *living* cardiac cells (Figure 3D).

At the beginning of the paper, we presented a master/slave behavior whereby a cell that strongly coupled mechanically to its neighbor (‘slave’) has low beat-to-beat variability as a consequence of the strong coupling and is following the average beating frequency of a highly stochastic cell (‘master’) that can barely detect its neighbor. This phenomenon raises intriguing questions. Can the steady state observed in Figure 1 be a consequence of a ‘noisy’ cell reducing the variability of a neighboring cell below its own variability? And can the ‘slave’ indeed be paced by the average frequency of a highly stochastic ‘master’? Using

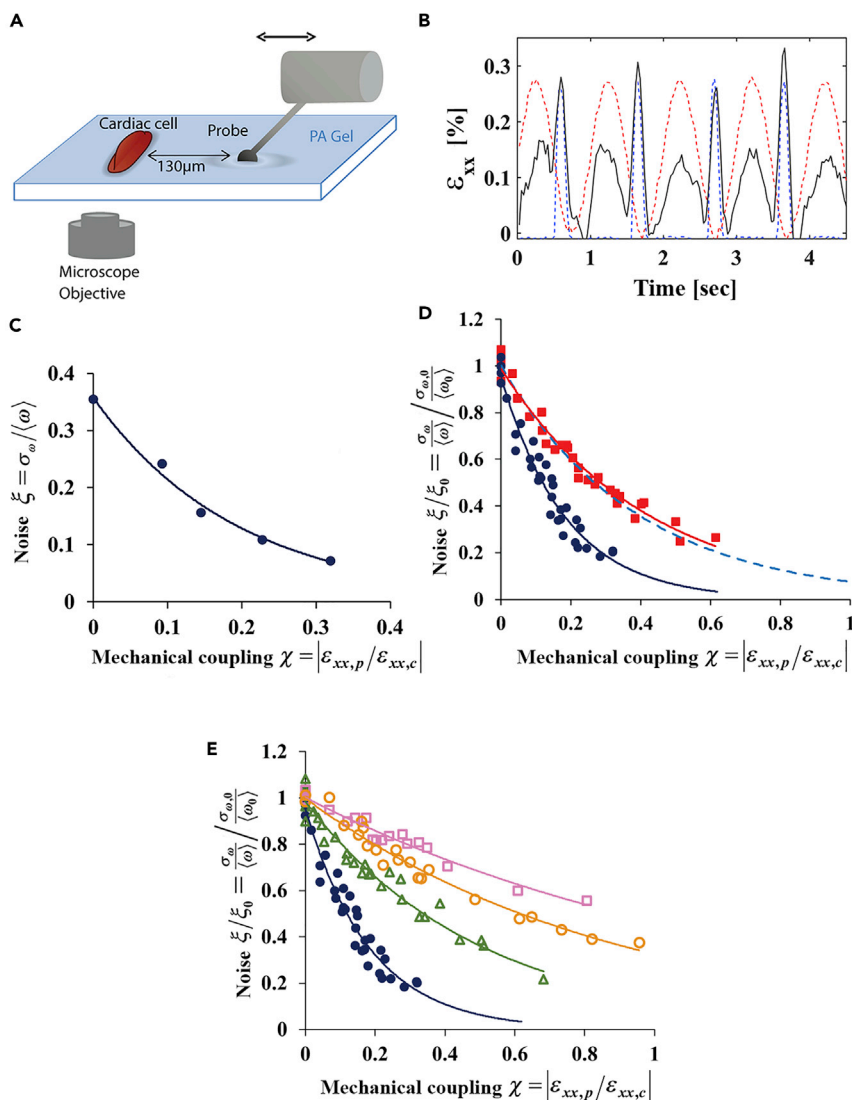


Figure 3. Noise Is Reduced Exponentially with Increased Mechanical Coupling to a ‘Mechanical Cell’

(A) A schematic representation of the ‘mechanical cell’ setup. A tungsten probe applies an oscillatory stretch that mimics the deformations generated by a beating cardiac cell.

(B) The deformations at the edge of the cell in the direction perpendicular to the contraction axis (black curve) are generated by both the cardiac cell and the mechanical probe. The probe oscillation signal is represented by the dashed red curve, and the cell beating signal is shown in the dashed blue curve. The mechanical coupling is defined as the ratio between the strain generated by the probe at the edge of the cell and the strain generated by the cell itself, $\chi = |\varepsilon_{xx,p} / \varepsilon_{xx,c}|$.

(C) The dependence of beating variability on the strength of mechanical interaction with a mechanical probe for a representative isolated beating cardiac cell.

(D) The dependence of beating variability, normalized to the beat-to-beat variability before probe activation, on the mechanical interaction with a deterministic mechanical probe (●, blue filled circles) or with a stochastic mechanical probe (■, red filled squares). The decay constant for the deterministic and stochastic probe are 5.5 ± 0.23 and 2.4 ± 0.11 , respectively. The blue dashed line represents the exponential fit for the decay of beating noise with mechanical coupling within pairs of aligned cardiac cells as shown in Figure 3B. For each cell, the probe amplitude was gradually increased and beating noise was monitored as a function of the strength of mechanical interaction. For each cell, we get an exponential decay similar to the curve shown in (C). After normalization of the beat-to-beat variability, ξ , by the beating variability of the isolated cell without mechanical interaction, ξ_0 (before probe activation), all the exponential decays converge to the same exponent. Probe frequency was equal to the average frequency of the beating cardiac cell to separate the effect of pacing a cardiac cell from that of noise reduction. The experiment with the deterministic and stochastic probes was repeated for $n = 11$ and $n = 6$ isolated beating cardiac cells, respectively.

Figure 3. Continued

(E) The dependence of beating variability, normalized to the beat-to-beat variability before probe activation, on the mechanical interaction with a deterministic mechanical probe with no drug (●, blue filled circles, decay constant: 5.5 ± 0.23 , $n = 11$), for cells treated with 10 μM Colchicine (Δ , green empty triangles, decay constant: 2.0 ± 0.1 , $n = 5$), 5 μM gp91-a NOX-2-specific inhibitor (○, orange empty circles, decay constant: 1.14 ± 0.05 , $n = 4$), 10 μM Autocamtide2-related inhibitory peptide (AIP), or CaMKII inhibitor (□, pink empty squares, decay constant: 0.77 ± 0.05 , $n = 4$). R^2 values for C–E are reported in Table S1 in the Supplemental Information. SDs were calculated using the bootstrap method.

a stochastic ‘mechanical cell’, we can reproduce the master-slave scenario in a setup where the master identity is well defined. The ‘mechanical cell’ cannot change as a result of interaction and therefore acts as a highly stochastic master. As clearly shown in Figure 4, using the stochastic probe we were able to pace an isolated beating cardiac cell to the average oscillation frequency of the probe as well as reduce its noise below that of the probe. Moreover, after mechanical stimulation stops, the new probe-induced beating frequency and the reduced noise level persist.

The observation that the reduction in noise persists after stimulation stops suggests that the forces involved in mechanical communication induce changes in the biochemical network kinetics that governs spontaneous beating in cardiac cells. It is supported further by the fact that the noise is reduced below the noise of the master probe.

Microtubule Integrity, CaMKII, and NOX-2 Are Involved in Mechanical Coupling-Induced Noise Reduction

The relatively long time (~ 10 minutes) required for noise reduction (Figure S6) and the observations that the reduction in noise persists after stimulation stops (Figures 4 and S6) and that noise is reduced below the noise of a master probe (Figure 4C) suggest that the forces involved in mechanical communication induce long-term alterations in cardiac cell spontaneous beating. Recently, it was shown that mechanical stretch triggers the production of reactive oxygen species that target Ca^{2+} signaling proteins (Prosser and Ward, 2014). This pathway was shown to often involve signaling through microtubule-dependent NADPH oxidase 2 (NOX2) and CaMKII that regulate RyR2 kinetics (Prosser and Ward, 2014; Prosser et al., 2011; Iribe et al., 2009; Jian et al., 2014 and Figure S7). To test whether this mechano-transduction pathway is involved in noise reduction, we repeated the probe assay in the presence of inhibitors for key proteins in this pathway. We again monitored beating noise as a function of the strength of mechanical interaction with the probe while gradually increasing the probe average amplitude. As shown in Figure 3E, treatment with either Colchicine, a microtubule polymerization inhibitor, or gp91ds-tat, a specific NOX-2 peptide inhibitor, interferes with beating noise reduction by mechanical coupling and reduces the decay constant from 5.5 ± 0.23 to 2.0 ± 0.1 or 1.14 ± 0.05 , respectively. The largest effect occurred with Autocamtide2-related inhibitory peptide (AIP), a CaMKII-specific inhibitor, which almost eliminated the reduction in beating noise (decay constant of 0.77 ± 0.05 , Figure 3E).

DISCUSSION

Here we show that mechanical communication reduces beat-to-beat variability. We directly measure mechanical coupling and show that the noise is reduced exponentially with the strength of mechanical coupling. We demonstrate this both in pairs of mechanically coupled beating cardiac cells and in a system in which an isolated beating cardiac cell interacts mechanically with an artificial ‘mechanical cell’. The significance of this phenomenon is clearly emphasized by the cardiac cell pair presented at the beginning of the paper. These cells are synchronized at their average beating frequency; however, since one of the cells is highly stochastic they go in and out of phase. This demonstrates that noise reduction is essential to achieve synchronized phase of beating. In this paper, we studied noise reduction in spontaneously beating cells in culture. Most cells in the heart do not beat spontaneously but are paced by an electrical signal generated by pacemaker cells. However, pacemaker cells themselves beat spontaneously. Pacemaker cell beating variability is determined by the stochasticity of the biochemical network that underlies spontaneous beating (Yaniv et al., 2014). Mechanical communication may therefore be involved in the regulation of beat-to-beat variability in spontaneously beating pacemaker cells in the sinoatrial (SA) node and in synchronized pacemaker activity. In addition, mechanical communication may play a significant role in synchronized contractions during the

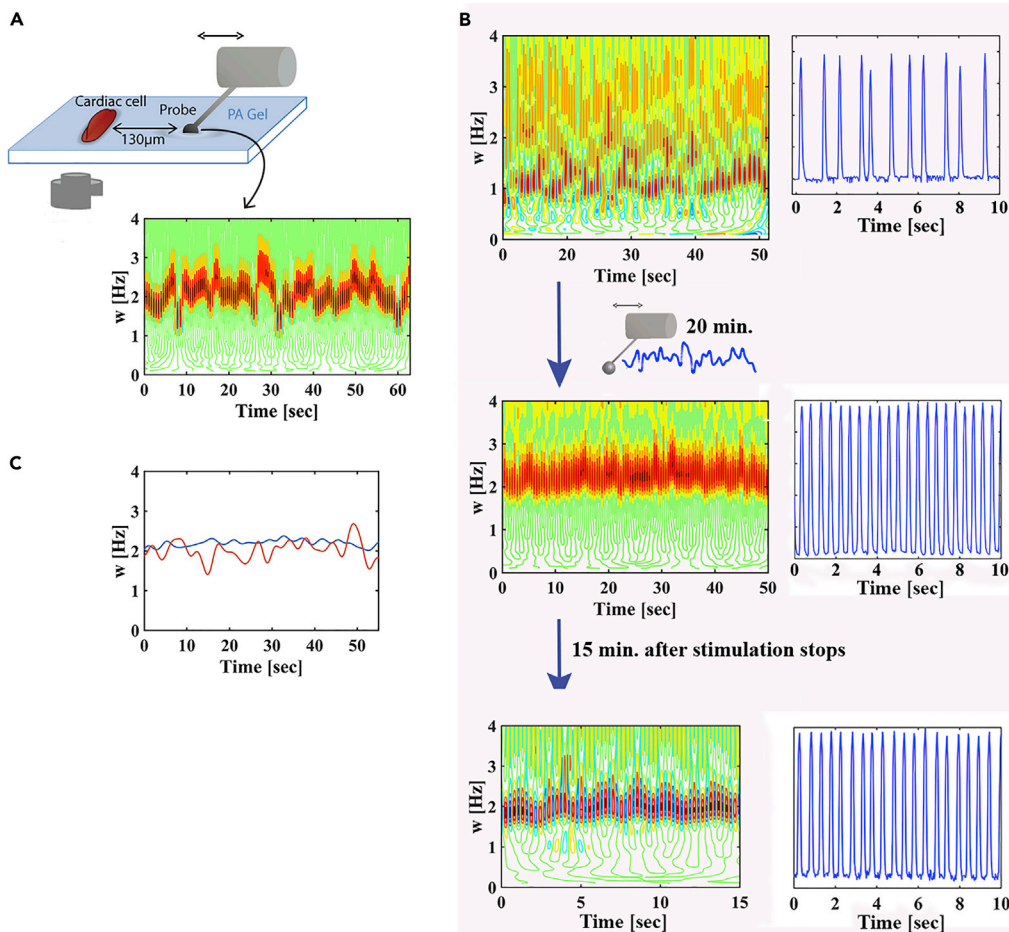


Figure 4. Pacing and Noise Reduction of an Isolated Spontaneously Beating Cardiac Cell Using a Stochastic 'Mechanical Cell'

(A) The signal generated by a stochastic 'mechanical cell' as extracted from a wavelet analysis. Probe frequencies were generated from a Gaussian distribution with an average of 2 Hz and an SD of 0.25 Hz. The mechanical coupling with the probe in this experiment was $\chi = 0.305$. This experiment was repeated for $n = 4$ cells.

(B) Frequency as a function of time (left) and normalized beating signal over time (right), before mechanical stimulation (top), after 30 min of mechanical interaction with a stochastic mechanical probe (middle), and 15 min after stimulation stops (bottom). The cell initially beats at 1 Hz with a beat-to-beat variability of $\xi = 0.4$; after mechanical stimulation with a stochastic probe, the cell is paced to 2 Hz with a beat-to-beat variability of $\xi = 0.05$, lower than that of the mastering probe. These values persist after stimulation stops.

(C) The frequency of the probe (red) and of the cardiac cell (blue) in a short time window of ~ 1 min after 30 min of training.

development of the heart in early stages where electrical conduction is not fully functional (Chiou et al., 2016).

Our results indicate that the mechanism behind mechanical communication-induced noise reduction in our system requires enzymatic activity (NOX2 and CaMKII) in a pathway that was shown to regulate RyR2 kinetics (Prosser et al., 2011). To provide a possible explanation for the necessity of CaMKII activity for the reduction in noise, we would like next to discuss how changes to enzymatic activity could lead to reduced noise levels. We showed that inhibiting CaMKII interferes with noise reduction by mechanical communication. In a linear pathway (such as the one shown in Figure S7 and discussed in the literature for cardiac cell mechanosensing, which is consistent with our data), it means that CaMKII is activated by the mechanical signal (i.e., its activity is increased). For this reason, in our possible explanation we will consider how increased enzymatic activity can regulate noise in a biochemical network.

To do so, it is instructive to begin with a ‘thought experiment’. Consider a reversible reaction between two states, for example, the phosphorylated and dephosphorylated states of RyR. For simplicity, let us first think about this reaction as a simple isomerization reaction, i.e., $RyR \xrightleftharpoons[k_{off}]{k_{on}} RyR_P$, where k_{on} and k_{off} are the rate constants for phosphorylation/dephosphorylation and will therefore depend on the concentration of kinase/phosphatase, respectively. Increased activity of both the kinase and phosphatase will multiply k_{on} and k_{off} by an identical factor. Therefore, in this case, at equilibrium the fraction of phosphorylated RyR will be the same. However, when the activity of the kinase and phosphatase is higher, the transition between the two states will be faster. Suppose now that we measure the average fraction of phosphorylated channels in ‘sampling windows’ of size Δt . The width of the distribution of measured average fraction values is the effective noise in the system (Figure S8C). If the kinetics is faster than Δt , during this time interval, the channel will go back and forth between phosphorylated and dephosphorylated states, essentially sampling the full equilibrium distribution within each ‘sampling window’. In this case, the average fraction measured in every sampling window is nearly identical (Figures S8B and S8C). Faster kinetics, therefore, reduces system noise as measured by the average fraction of RyR_P at discrete sampling windows. The frequency of calcium oscillations is determined by the kinetics of RyR channels, which depends on their phosphorylation state. The cell essentially “samples” the RyR_P distribution, and therefore, faster kinetics, which leads to low variability in the fraction of phosphorylated channels, will reduce the beat-to-beat variability. To demonstrate that noise reduction by increased enzyme activity (e.g., CaMKII) may occur through cardiac cells ‘sampling’ of phosphorylated RyR channel distribution, we conducted a stochastic kinetic simulation of a cardiac cell. Full details can be found in the [Supplemental Information \(Data S1 and Figure S9\)](#). It is important to note that this idea of how modulating enzymatic activity can regulate noise is not limited to cardiac cells. Indeed, the regulation of enzymatic activity can regulate noise in any biochemical network.

We show here directly that mechanical coupling regulates intrinsic noise in cardiac cell beating and that noise reduction by mechanical coupling is sensitive to the stochastic nature of the master cell. It is very likely that our observations extend beyond this specific biological system and that mechanical coupling also regulates intrinsic noise in other cellular systems in which mechanical communication is of importance.

Limitation of the Study

In the simulation presented in the discussion, we do not address mechanical coupling between cells. Mechanical communication is only taken into account as an increased activity of a RyR kinase (e.g., CaMKII). We use the model to discuss possible explanation for how increased enzymatic activity can regulate noise in a biochemical network. Further work is required to elucidate the detailed mechanism underlying mechanical communication-mediated noise reduction.

METHODS

All methods can be found in the accompanying [Transparent Methods supplemental file](#).

DATA AND SOFTWARE AVAILABILITY

The accession number for the raw data reported in this paper is <https://doi.org/10.17632/djrdcbdrn8.1>.

SUPPLEMENTAL INFORMATION

Supplemental Information can be found online at <https://doi.org/10.1016/j.isci.2019.02.030>.

ACKNOWLEDGMENTS

We thank Dr. Ruth Hershberg for comments that greatly improved the manuscript. We also thank Dr. Khaled Gommed for help with microfabrication. This work was supported by the Israel Science Foundation grants 591/14, 507/18 and 1880/14.

AUTHOR CONTRIBUTIONS

S.T. designed research and wrote the manuscript. H.V., I.N., and S.D. performed experiments; H.V., I.N., and S.T. analyzed the data; L.S. performed computer simulations; S.T. supervised the research. All authors discussed and helped prepare the manuscript.

DECLARATION OF INTERESTS

The authors declare no competing interests.

Received: June 27, 2018

Revised: December 29, 2018

Accepted: February 26, 2019

Published: April 26, 2019

REFERENCES

- Angelini, T.E., Hannezo, E., Treppe, X., Fredberg, J.J., and Weitz, D.A. (2010). Cell migration driven by cooperative substrate deformation patterns. *Phys. Rev. Lett.* *104*, 168104.
- Chiou, K.K., Rocks, J.W., Chen, C.Y., Cho, S., Merkus, K.E., Rajaratnam, A., Robison, P., Tewari, M., Vogel, K., Majkut, S.F., et al. (2016). Mechanical signaling coordinates the embryonic heartbeat. *Proc. Natl. Acad. Sci. U S A* *113*, 8939–8944.
- Cohen, O., and Safran, S.A. (2016). Elastic interactions synchronize beating in cardiomyocytes. *Soft Matter* *12*, 6088–6095.
- Engler, A.J., Griffin, M.A., Sen, S., Bönnemann, C.G., Sweeney, H.L., and Discher, D.E. (2004). Myotubes differentiate optimally on substrates with tissue-like stiffness. pathological implications for soft or stiff microenvironments. *J. Cell Biol.* *166*, 877–887.
- Engler, A.J., Carag-Krieger, C., Johnson, C.P., Raab, M., Tang, H.Y., Speicher, D.W., Sanger, J.W., Sanger, J.M., and Discher, D.E. (2008). Embryonic cardiomyocytes beat best on a matrix with heart-like elasticity: scar-like rigidity inhibits beating. *J. Cell Sci.* *121*, 3794–3802.
- Heijman, J., Zaza, A., Johnson, D.M., Rudy, Y., Peeters, R.L.M., Volders, P.G.A., and Westra, R.L. (2013). Determinants of beat-to-beat variability of repolarization duration in the canine ventricular myocyte: a computational analysis. *PLoS Comput. Biol.* *9*, e1003202.
- Hinczewski, M., and Thirumalai, D. (2014). Cellular signaling networks function as generalized wiener-Kolmogorov filters to suppress noise. *Phys. Rev. X* *4*, 041017.
- Iribe, G., Ward, C.W., Camelliti, P., Bollensdorff, C., Mason, F., Burton, R.A.B., Garry, A., Morphew, M.K., Hoenger, A., Lederer, W.J., and Peter, K. (2009). Axial stretch of rat single ventricular cardiomyocytes causes and acute and transient increase in Ca²⁺ spark rate. *Circ. Res.* *104*, 787–795.
- Jian, Z., Han, H., Zhang, R., Puglisi, J., Izu, L.T., Shaw, J.A., Onofriok, E., Erickson, J.R., Chen, Y.J., Horvath, B., et al. (2014). Mechanochemotransduction during cardiomyocyte contraction is mediated by localized nitric oxide signaling. *Sci. Signal.* *7*, ra27.
- Lakatta, E.G., Maltsev, V.A., and Vinogradova, T.M. (2010). A coupled system of intracellular Ca²⁺ clocks and surface membrane voltage clocks controls the timekeeping mechanism of the Heart's Pacemaker. *Circ. Res.* *106*, 659–673.
- Majkut, S., Idema, T., Swift, J., Krieger, C., Liu, A., and Discher, D.E. (2013). Heart-specific stiffening in early embryos parallels matrix and myosin expression to optimize beating. *Curr. Biol.* *23*, 2434–2439.
- Maltsev, V.A., and Lakatta, E.G. (2009). Synergism of coupled subsarcolemmal Ca²⁺ clocks and sarcolemmal voltage clocks confers robust and flexible pacemaker function in a novel pacemaker cell model. *Am. J. Physiol. Heart Circ. Physiol.* *296*, H594–H615.
- Nitsan, I., Drori, S., Lewis, Y.E., Cohen, S., and Tzliil, S. (2016). Mechanical communication in cardiac cell synchronized beating. *Nat. Phys.* *12*, 472–477.
- Prosser, B.L., and Ward, C.W. (2014). Mechanochemo transduction tunes the heartstrings. *Sci. Signal.* *7*, pe7.
- Prosser, B.L., Ward, C.W., and Lederer, W.J. (2011). X-ROS signaling: rapid mechanochemo transduction in heart. *Science* *333*, 1440–1445.
- Quinn, T.A., and Kohl, P. (2012). Mechano-sensitivity of cardiac pacemaker function: pathophysiological relevance, experimental implications, and conceptual integration with other mechanisms of rhythmicity. *Prog. Biophys. Mol. Biol.* *110*, 257–268.
- Rackauckas, C., Schilling, T., and Nie, Q. (2018). Mean-independent noise control of cell fates via intermediate states. *iScience* *3*, 11–20.
- Reinhart-King, C.A., Dembo, M., and Hammer, D.A. (2008). Cell-cell mechanical communication through compliant substrates. *Biophys. J.* *95*, 6044–6051.
- Sapir, L., and Tzliil, S. (2017). Talking over the extracellular matrix: how do cells communicate mechanically? *Semin. Cell Dev. Biol.* *71*, 99–105.
- Tang, X., Bajaj, P., Bashir, R., and Saif, T.A. (2011). How far cardiac cells can see each other mechanically. *Soft Matter* *7*, 6151–6158.
- Winer, J.P., Oake, S., and Janmey, P.A. (2009). Non-linear elasticity of extracellular matrices enables contractile cells to communicate local position and orientation. *PLoS One* *4*, e6382.
- Yang, H.T., Tweedie, D., Wang, S., Guia, A., Vinogradova, T., Bogdanov, K., Allen, P.D., Stren, M.D., Lakatta, E.G., and Boheler, K.R. (2002). The ryanodine receptor modulates the spontaneous beating rate of cardiomyocytes during development. *Proc. Natl. Acad. Sci. U S A* *99*, 9225–9230.
- Yaniv, Y., Lyashkov, A.E., Sirenko, S., Okamoto, Y., Guiriba, T.-R., Ziman, B.D., Morrell, C.H., and Lakatta, E.G. (2014). Stochasticity intrinsic to coupled-clock mechanisms underlies beat-to-beat variability of spontaneous action potential firing in sinoatrial node pacemaker cells. *J. Mol. Cell. Cardiol.* *77*, 1–10.

ISCI, Volume 14

Supplemental Information

Mechanical Communication

Acts as a Noise Filter

Hen Viner, Ido Nitsan, Liel Sapir, Stavit Drori, and Shelly Tzvil

Transparent Methods

All laboratory procedures conform to the Guide for the Care and Use of Laboratory Animals published by the U.S. National Institutes of Health. Animal usage was approved by the Animal Care and Use Committee of the Technion, Israel Institute of Technology.

PDMS stamp: microfabrication and soft lithography: The patterns were designed using CleWin 5 (PhoeniX Software, NL). Isolated pairs of rectangles were designed. Rectangles were either 20 x 50um or 20 x 100um. Each rectangle represents a place that will be occupied by a cardiac cell. The distance between two cells in each pair varies throughout the mask (e.g. 10, 20, 40, 80, 120um). Chrome masks were manufactured by Delta Mask (Delta Masks BV, NL). A Si master with geometric patterns was fabricated using standard photolithographic technique as previously described (Tang et al., 2012). PDMS prepolymer was obtained via mixing Silicone elastomer and curing agent at 10:1 ratio (Dow Corning, Midland, MI) and degassing the mixture in a desiccator for 30 min. The prepolymer solution was poured over the Si master mold and cured in the oven at 80°C for 2 h. The elastomeric stamp was then peeled off carefully and cut in 1 × 1 cm² squares for micropatterning.

Intermediate patterned glass coverslips: Either Matrigel or laminin (Corning Inc, NY) was diluted 1:10 in L15 medium (Thermo Fisher). 160μl of the solution was added to the top of elastomeric microstamps, and incubated at 4°C overnight. Following incubation, the solution was aspirated, and the surface of the stamps was dried with a low stream of N₂ gas. The stamps were then used to micropattern clean glass coverslips, via microcontact printing. The stamp was brought into complete conformal contact with a glass coverslip substrate for 5min at room temperature. Small weights (38 g) were placed over the PDMS stamp to aid complete protein pattern transfer from PDMS to intermediate glass (Tang et al., 2012).

Patterned polyacrylamide plates: Polyacrylamide (PA) gel coated plates were prepared following the protocol described previously (Nitsan et al., 2016). Briefly, 30mm glass bottom plates (Greiner, Austria) were activated using 2% 3-aminopropyltrimethoxysilane and 1% glutaraldehyde solution. Polyacrylamide/Bis-acrylamide 7.5/0.03% solution was mixed with 0.02% suspension of carboxylated dark red fluospheres (Life Technologies), 0.05% Ammonium Persulfate and 0.4% Temed (Bio-Rad, CA). 7.5 μ l of mixed PA solution was applied on each activated plate and covered with, matrigel patterned glass coverslip, to form a thin film. The patterned matrigel on the coverslips was transferred to the surface of the polyacrylamide substrates during gelation. Films were left to polymerize for 30 min in room temperature. Following polymerization, polyacrylamide substrates were incubated in phosphate-buffered saline for at least 1 h and the top coverslips were carefully removed with a razor blade (Ribeiro et al., 2015).

Cell Culture: Neonatal cardiomyocytes were isolated from zero-day-old Sprague Dawley (SD) rat pups using the Neonatal Cardiomyocyte Isolation System (Worthington, NJ) according to the manufacturer's instructions as described before (Nitsan et al., 2016). Briefly, hearts were rinsed with ice-cold HBSS and trypsinized for 16 hours at 4°C. Following trypsinization, hearts were incubated with trypsin inhibitor at 37°C, and then with collagenase solution for 30 minutes. Cells were triturated, pelleted and resuspended in L15 media (Worthington, NJ). Cells were then subjected to Percoll gradient for separation of cardiomyocytes from non-myocytes. Isolated cardiomyocytes were resuspended with culture media: F10 media (Sigma-Aldrich, MO) supplemented with 5% fetal calf serum (Biological-Industries, Israel), 5% donor horse serum (Life-technologies, CA), penicillin 10u/ml, streptomycin 0.1mg/ml, 5-Bromo-2'-deoxyuridine (5-BrdU) 0.05mg/ml and CaCl₂ 1mM (Sigma-Aldrich, MO). Cultured cardiomyocytes were grown for at least 72 hours and up to 6 days. Approximately 8×10^5 cells were plated on 30mm glass bottom

plates (Greiner, Austria) covered with either matrigel/laminin patterned PA gel. Noise reduction as a function of mechanical interaction with a mechanical probe was analyzed in the presence and absence of 10 μ M Colchicine (Sigma-Aldrich), 5 μ M gp91 ds – tat or 10 μ M Autocamtide - 2 - Related Inhibitory Peptide (AIP) (AnaSpec Fermont, Ca)

Spinning disc confocal microscopy: Imaging was done using a Nikon Ti-E inverted microscope equipped with two Evolve EMCCD cameras (Photomatrix), 4 laser lines (405,491,561,642), phase contrast and Yokagawa spinning disc confocal. The dish was maintained at 37 °C with 5% CO₂/95% air using a cage incubator (Okolab). Imaging was done using 40x 0.95 NA (air) PlanApo Lambda objective (Nikon). Fluorospheres were excited using 642nm laser (Vortran) and Lifeact-RFP was excited with 561nm laser (Cobolt). Lifeact imaging was done using 100x 1.49 NA oil objective (Nikon).

Visualization of F-Actin in cultured myocytes: 24h following plating cells were transduced with 100 MOI rAV^{CMV}-LifeAct-TagRFP (ibidi, Germany).

Mechanical probe: A rigid Tungsten probe with 25 μ m tip diameter (Signatone) was mounted on a three axes (X-Y-Z) micro-positioning stages (Thorlabs) installed on a custom made adaptor for the microscope stage. The probe's tip is immersed into the culture medium and slightly indents the PA substrate (2 μ m indentation) 130 μ m away from the target cell as previously described (Nitsan et al., 2016).

Data analysis. Basic image analysis is done using ImageJ and custom-written matlab codes. Mechanical deformations were analyzed using a Digital image processing (DIC) code (Jones, 2013).

Quantifying mechanical coupling: To quantify the level of mechanical coupling between a cardiac cell and its neighbor, or alternatively, to determine how strong can a beating cell sense the deformations generated by its neighbor, we define a mechanical coupling parameter, χ .

Cell beating on a flexible substrate generates deformations in the direction perpendicular to the contraction axis (x-axis) in addition to the ones in the direction of contraction (y-axis) due to the Poisson's effect (Fig. 1e-f and Fig.S2b-S3b). However, as clearly shown in the strain maps, the strain in the y-direction decays fast along the x-axis and most of the strain that is detected near the neighboring cell is in the x-direction. That fact also led us to mimic the deformations generated by a beating cell by oscillating the mechanical probe along the x-direction (Nitsan et al., 2016).

The edge of a beating cardiac cell undergoes deformations in the direction parallel to the contraction axis (y-axis) as well as in the perpendicular direction (x-axis). The strain in the y-direction of contraction originate almost solely from cell contraction, while both the cell and its neighbor (a living cardiac cell or a 'mechanical cell') contribute to the strain in the x-direction.

The neighboring cell is expected to have a significant influence when its deformations are on the same order of magnitude or higher than the ones generated by the cell itself. We therefore define mechanical coupling as the ratio between the deformations generated by a neighboring cell at the cell edge and those generated by the beating cell itself. More formally, we define , $\chi = \left| \varepsilon_{xx,n} / \varepsilon_{xx,c} \right|$

where $\varepsilon_{xx,n}$ is the strain generated by the neighboring cell along the vector connecting the two cells (x-axis) and $\varepsilon_{xx,c}$ is the strain generated by the cell itself. For example, in the case of a pair of beating cardiac cells, the mechanical coupling parameter for the left cell is defined as:

$\chi_L = \left| \varepsilon_{xx,R}(x=L) / \varepsilon_{xx,L}(x=L) \right|$, where $\varepsilon_{xx,R}(x=L)$ is the strain generated by the right cell in the x-direction at the edge of the left cell and $\varepsilon_{xx,L}(x=L)$ is the strain generated by the left cell in the x-

direction at its boundary. In a similar way, the mechanical coupling parameter for the right cell is defined as: $\chi_R = \left| \varepsilon_{xx,L}(x=R) / \varepsilon_{xx,R}(x=R) \right|$.

The location of the edge of the cell can be extracted directly from the strain field and it is consistent with phase contrast microscopy images (Fig. S2).

Although, cells that are mechanically coupled are synchronized and beat with similar average beating frequency, the finite variability results in periods of phase and anti-phase contractions. To be able to separate between the strain generated by the cell itself and by its neighbor, we use time periods where the cells beat in anti-phase as explained in detail in Fig. S3 and shown in Fig. S2a-S3a.

AFM. Force curves were collected on JPK NanoWizard3 atomic force microscope. A silicon nitride cantilever with an attached 600nm diameter SiO₂ particle tip (Novascan, Ames, IA) was used to indent samples for collecting force curves. The spring constant of the cantilever was calculated to be 0.25 N/m.

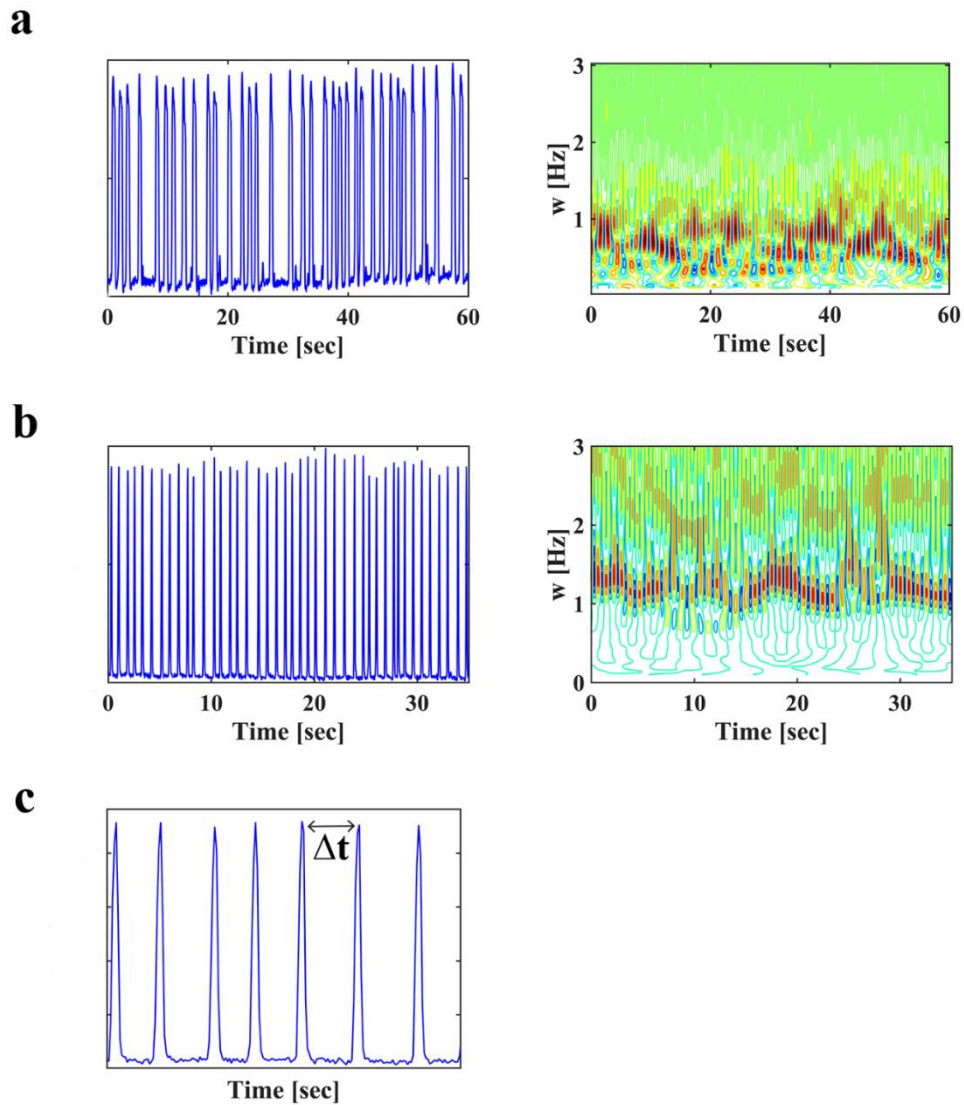


Figure S1: Beat-to-beat variability of an isolated spontaneously beating cardiac cell, related to Figure 1: a, b: two representative examples for the beating signal of a spontaneously beating isolated cardiac cell. *left:* Normalized beating signals over time, *right:* Beating frequency over time calculated using wavelet analysis (right). Beat-to-beat variability is defined either as the relative standard deviation of the frequency (ξ_ω) or as the relative standard deviation of the time between consecutive contractions, Δt defined in **c**, ($\xi_{\Delta t}$). According to these measurements, the noise for

the cell presented in **a** is: $\xi_{\omega} = 0.3$, $\xi_{\Delta t} = 0.35$. For the cell presented in **b** the values obtained are:

$$\xi_{\omega} = 0.19, \xi_{\Delta t} = 0.21.$$

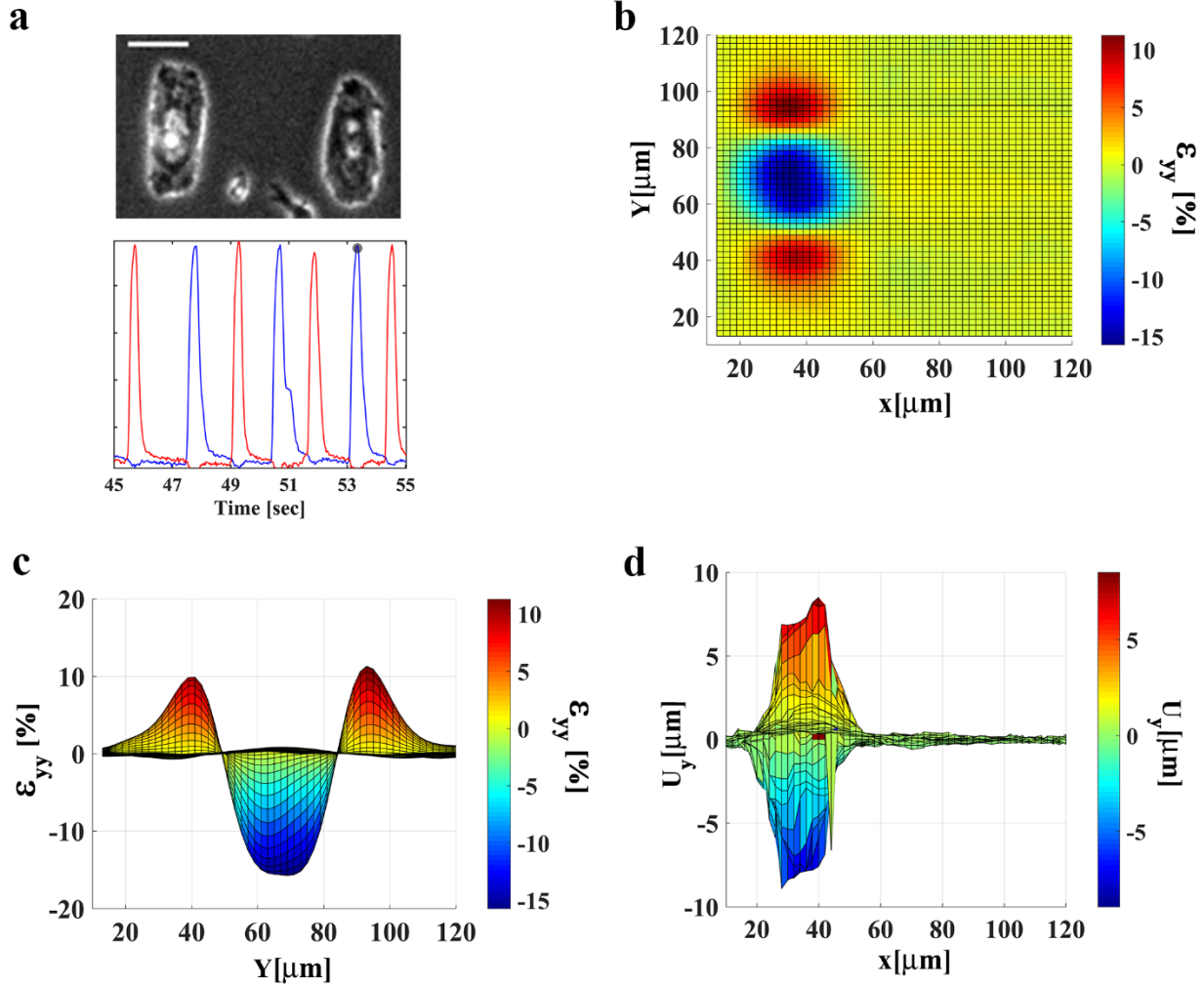


Figure S2: Cardiac cell dimension in the strain and displacement maps, related to Figure 2:

a: *top:* A pair of spontaneously beating cardiac cells. The scale bar is: $20\mu\text{m}$. *bottom:* A short time sequence where the cells beat in anti-phase. The blue and red curves are the normalized beating signals for the left and right cells respectively. **b,** Strain field map in the y -direction, $\varepsilon_{yy}(x, y)$ for a time point where the cells beat in anti-phase and only the left cell is contracting (the time point used is marked on a). The location of the contracting cell can be identified in the strain map as the

region where the strain in the y-direction is negative. **c**, a side view of the strain field shown in (b). The dimension of the contracting cell in the y-direction can be determined by the distance between the two zero points. **d**, A side view of the displacement field in the y-direction, $U_y(x, y)$. The width of the contracting cell (its dimension along the x-axis) can be determined by the length of the region with significant displacements.

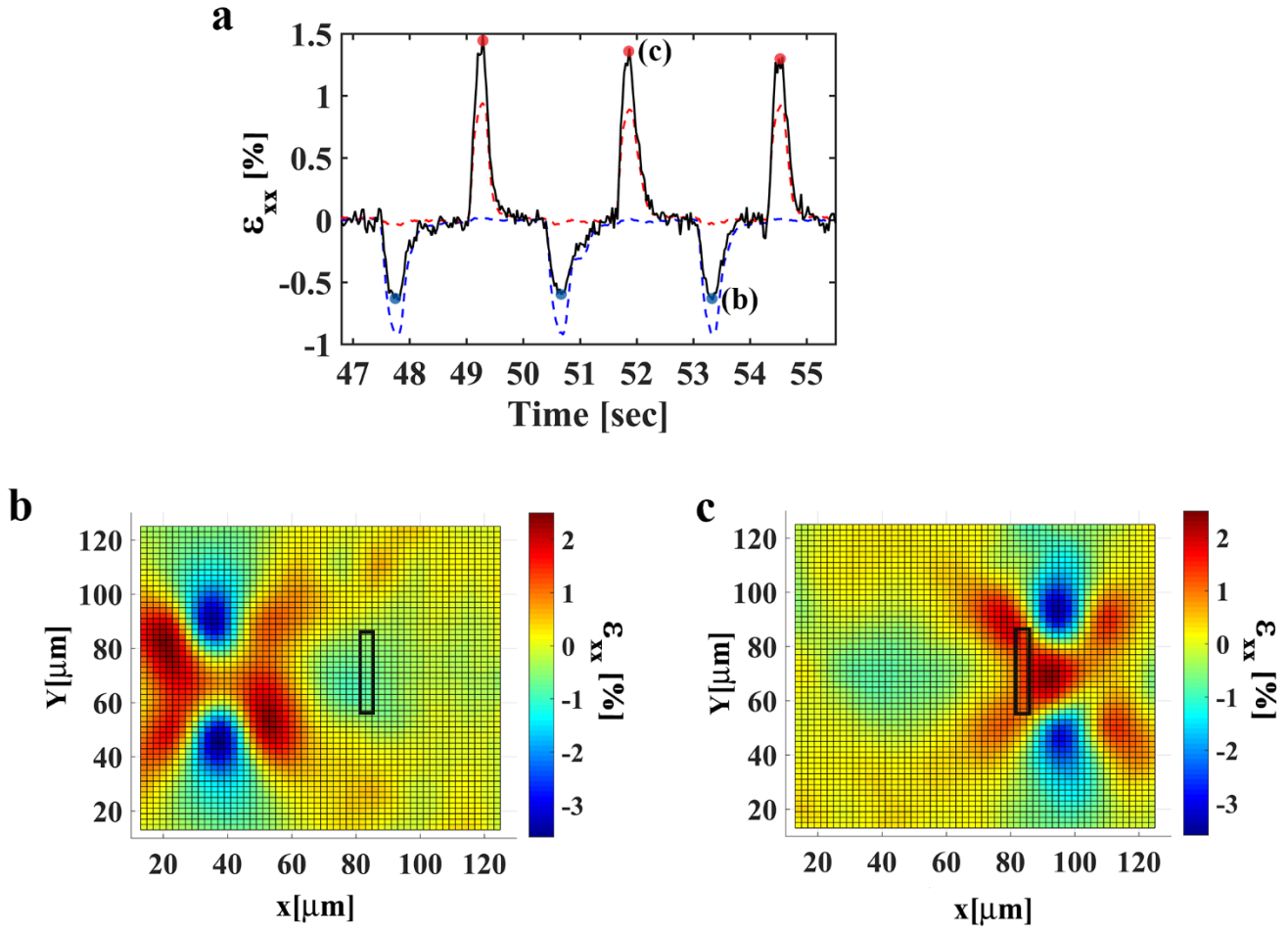


Figure S3: Calculating mechanical coupling, related to Figure 2: mechanical coupling is defined as the ratio between the deformations generated next to the beating cell by its neighbor and the deformations generated by the cell itself, $\chi = \left| \epsilon_{xx,n} / \epsilon_{xx,c} \right|$. **a:** the black curve shows the average strain at the edge of the right cell along the x-direction. The blue and red curves are the normalized beating signals of the left and right cells respectively (same as in Fig. S2a), and are only shown to mark the position of cell contraction. The strain peaks on the black curve marked with red dots result from contractions of the right cell, while the strain peaks marked with blue dots result from contractions of the left cell. **b,** Strain field map in the x-direction for time point (b) marked on the curve in (a), showing the strain field generated by the beating of the left cell. **c,**

Strain field map in the x-direction for time point (c) marked on the curve in (a), showing the strain field generated by the beating of the right cell. Mechanical coupling for the right cell, $\chi_R = \left| \varepsilon_{xx,L}(x=R) / \varepsilon_{xx,R}(x=R) \right|$ is estimated by dividing the average strain values generated by the left cell at the edge of the right cell (blue dots) by the average strain generated by the left cell next to its edge (red dots). As clearly shown in (b) and (c), the strain generated by the right cell next to its edge is positive, while the strain generated by the left cell at the edge of the right cell is negative. We therefore, define the absolute value of this ratio as mechanical coupling. For clarity, the position of the edge of the right cell is marked on the strain maps by a black rectangle.

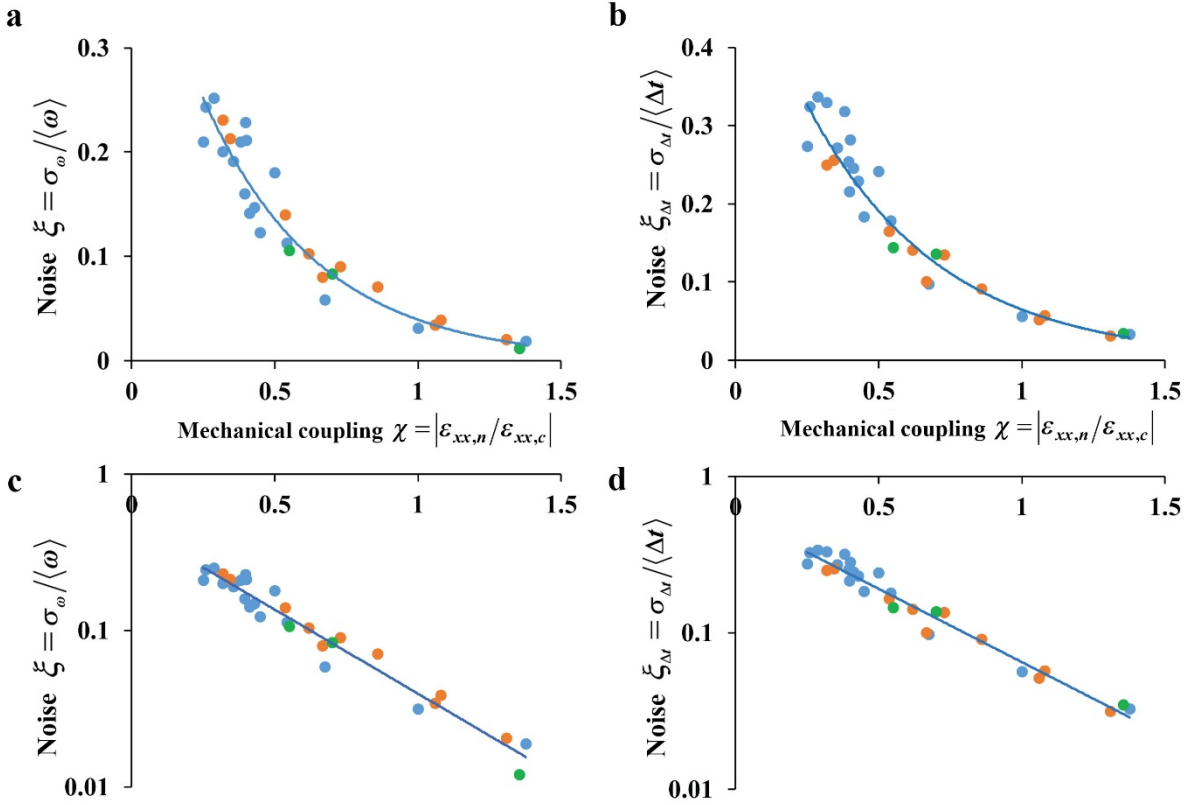


Figure S4: Data from cells cultured on different substrate rigidities and coatings can be combined, related to Figure 2. We repeated the experiment using pairs of cells cultured on a softer substrate (1kPa). Beating noise, defined as the standard deviation of the beating frequency (a and c) or as the relative standard deviation of the time between consecutive beatings (b and d), is plotted as a function of mechanical coupling. c and d show the noise in a logarithmic scale. The blue and orange circles represent cells that were cultured on matrigel-coated 4kPa and 1kPa substrates respectively. The green circles represent cells that were cultured on laminin-coated 4kPa substrate. Pairs cultured on laminin fall on the same exponential curve as the ones cultured on matrigel. This is to be expected since while substrate coating may influence adhesion morphology and therefore the level of deformations induced in the underlying substrate, the dependence on mechanical coupling will not change as we measure directly the effective coupling by quantifying the deformations generated in the substrate. n=30 cells are shown from 8 different cultures and 16

different dishes. The decay constants obtained for pairs of cells cultured on 4kPa substrate and 1kPa substrate are: 2.49 ± 0.3 and 2.45 ± 0.12 respectively when the noise was calculated as the relative standard deviation of the beating frequency $\xi_{\omega} = \sigma_{\omega} / \langle \omega \rangle$ and 2.27 ± 0.3 and 2.04 ± 0.13 respectively when the noise was calculated as the relative standard deviation of the time between consecutive contractions, $\xi_{\Delta t} = \sigma_{\Delta t} / \langle \Delta t \rangle$. Standard deviations were calculated using the bootstrap method. No statistical significant difference was found between the exponential curves obtained using either the cells cultured on the 4kPa substrate or the ones cultured on 1kPa substrates. The decay constant for the total population is 2.43 ± 0.19 for ξ_{ω} and 2.2 ± 0.14 for $\xi_{\Delta t}$. To test the convergence of the exponential model, we used leave-one-out-cross-validation. For each test point, the error was within the standard deviation of the training set.

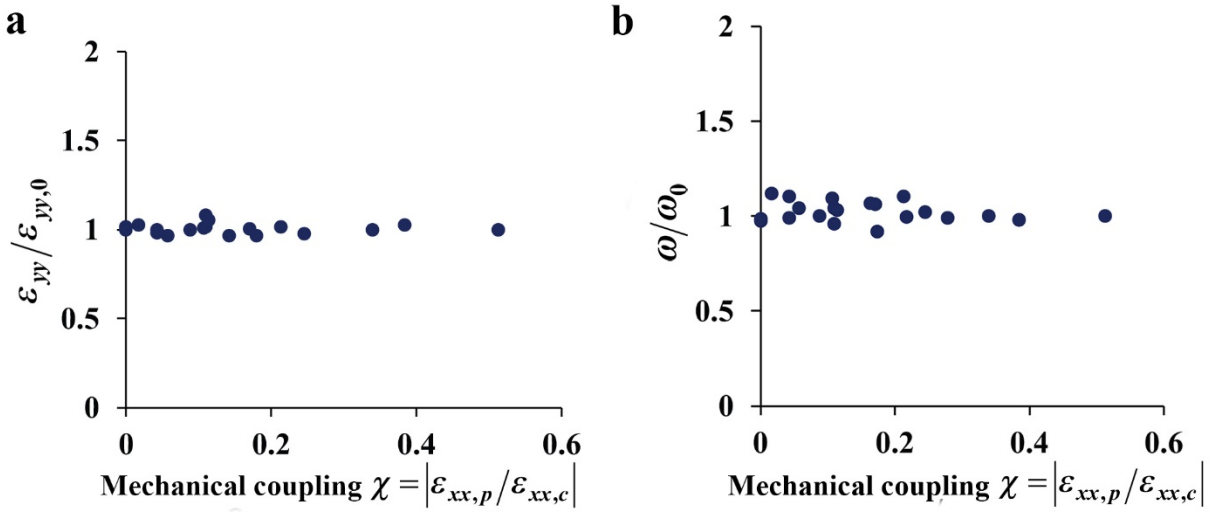


Figure S5: Filtering noise does not affect cell beating frequency or beating amplitude, related to Figure 3: Probe amplitude was gradually increased. In each amplitude, we let the cell interact with the probe for 10 minutes before recording the signal and increasing the amplitude to allow the cell to reach stationary behavior. Probe frequency was set equal to the average frequency of the beating cardiac cell in order to separate the effect of pacing a cardiac cell from that of noise reduction. **a:** The average strain generated by the cell along its long axis, normalized to its value prior to probe activation as a function of the level of mechanical coupling to a mechanical probe. **b:** The beating frequency, normalized to the frequency prior to probe activation as a function of the level of mechanical coupling to a mechanical probe. n=5 representative cells are shown.

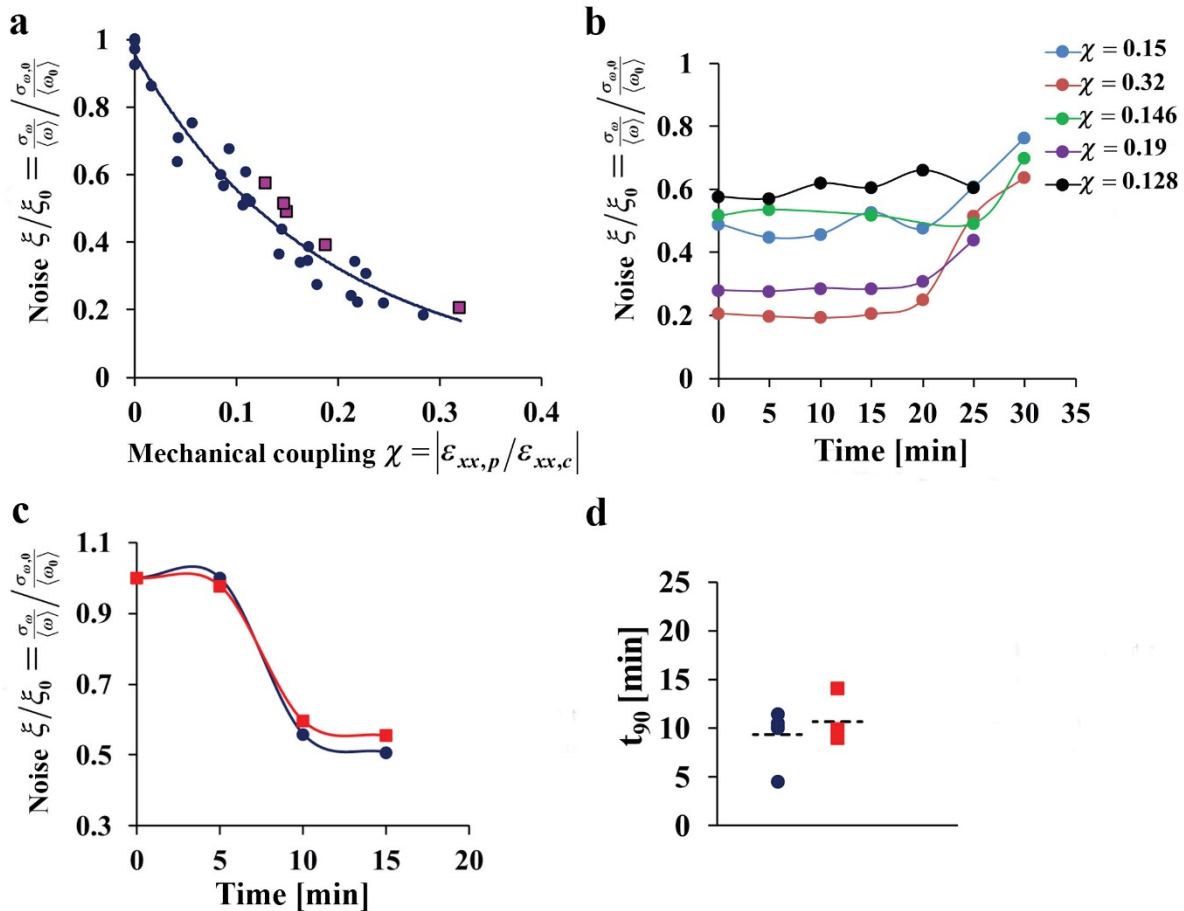


Figure S6: Time course of beating noise reduction with mechanical interaction with a ‘mechanical cell’, related to Figure 3: **a:** The dependence of beating variability, normalized to the beat-to-beat variability prior to probe activation, on the mechanical interaction with a mechanical probe without noise (deterministic). We conducted two versions of the experiment. In the first version (●, blue filled circles), probe amplitude was gradually increased. In each amplitude, we let the cell interact with the probe for 10 minutes before recording the signal and increasing the amplitude to allow the cell to reach stationary behavior. In order to find the time scale required to reach stationary behavior, we conducted a different version of the experiment. We let each cell interact with the probe in a single amplitude for a longer time, of the order of 40 minutes (■, purple filled squares) before mechanical stimulation is stopped. During that time,

beating noise was monitored in 5 minutes intervals. The cells marked by purple filled squares (■) were used in **b** and **d**. **b**: Representative curves for the beating noise after mechanical stimulation stops ($t=0$). The mechanical coupling parameter for each cell is marked in the figure. The reduction in beating noise persists after mechanical stimulation stops. The persistent time did not show a dependence on the level of mechanical coupling **c**: Representative curves for the time course of beating noise reduction. ($t=0$, mechanical probe is activated) are shown for a cell interacting with a deterministic probe (●, blue filled circles) and a stochastic probe (■, red filled squares) respectively. **d**: The time required for 90% beating noise reduction (t_{90}) for a cell interacting with a deterministic probe (●, blue filled circles) or a stochastic probe (■, red filled squares) respectively. The average time is marked by a dashed line. No significant difference for the time required for 90% beating noise reduction was found when a cell interacts mechanically with either a stochastic or a deterministic probe (10.6 ± 1 and 9.3 ± 1.1 respectively).

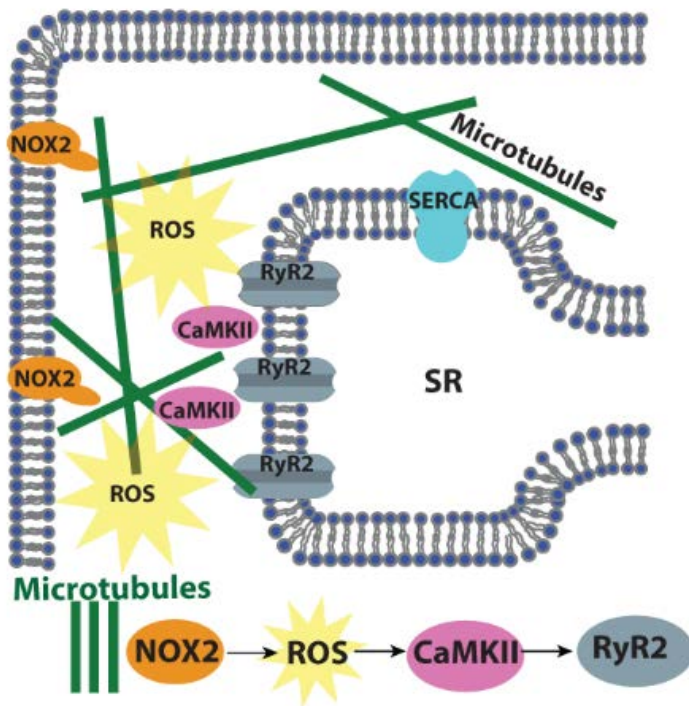


Figure S7: Schematic illustration of the mechanotransduction pathway discussed in the literature, related to Figure 3: Schematic illustration of the mechanotransduction pathway described in (Prosser and Ward, 2014). To test whether this mechanotransduction pathway is involved in noise reduction, we repeated the probe assay in the presence of inhibitors for key proteins in this pathway (Fig. 3e).

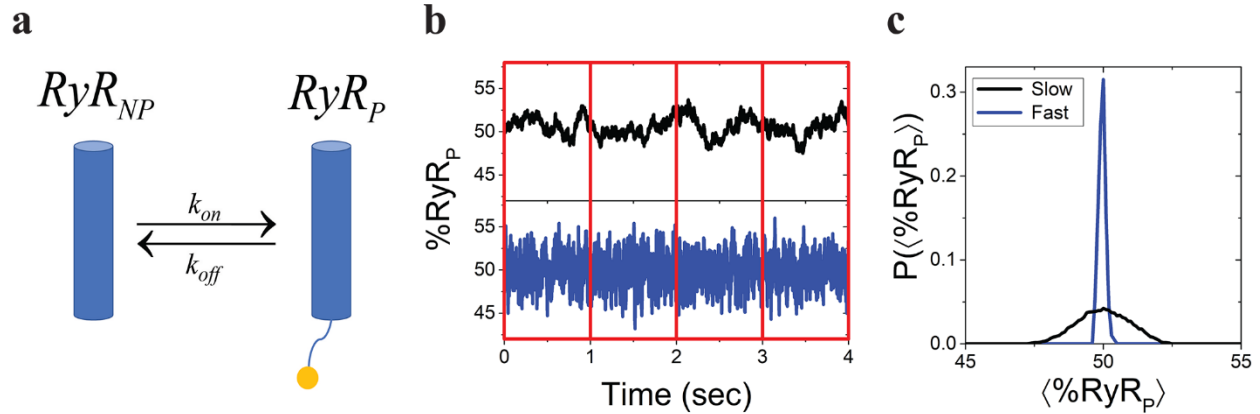


Figure S8. Noise reduction in reversible isomerization, related to DataS1. **a:** Schematic representation of phosphorylation/dephosphorylation of RyR2 modeled as a reversible isomerization reaction. **b:** Time evolution of the fraction of ‘phosphorylated RyR’, $\%RyR_P$, for slow kinetics (top), and faster kinetics (bottom) for 1000 molecules. The red rectangles represent sampling time windows. **c:** The sampling distribution of the average fraction of ‘phosphorylated RyR’ $\langle \%RyR_P \rangle$. Faster kinetics results in a narrow distribution of the values of the average fraction of ‘phosphorylated RyR’ as sampled in different sampling windows. The calculation was conducted using the SSA algorithm as discussed in Data S2.

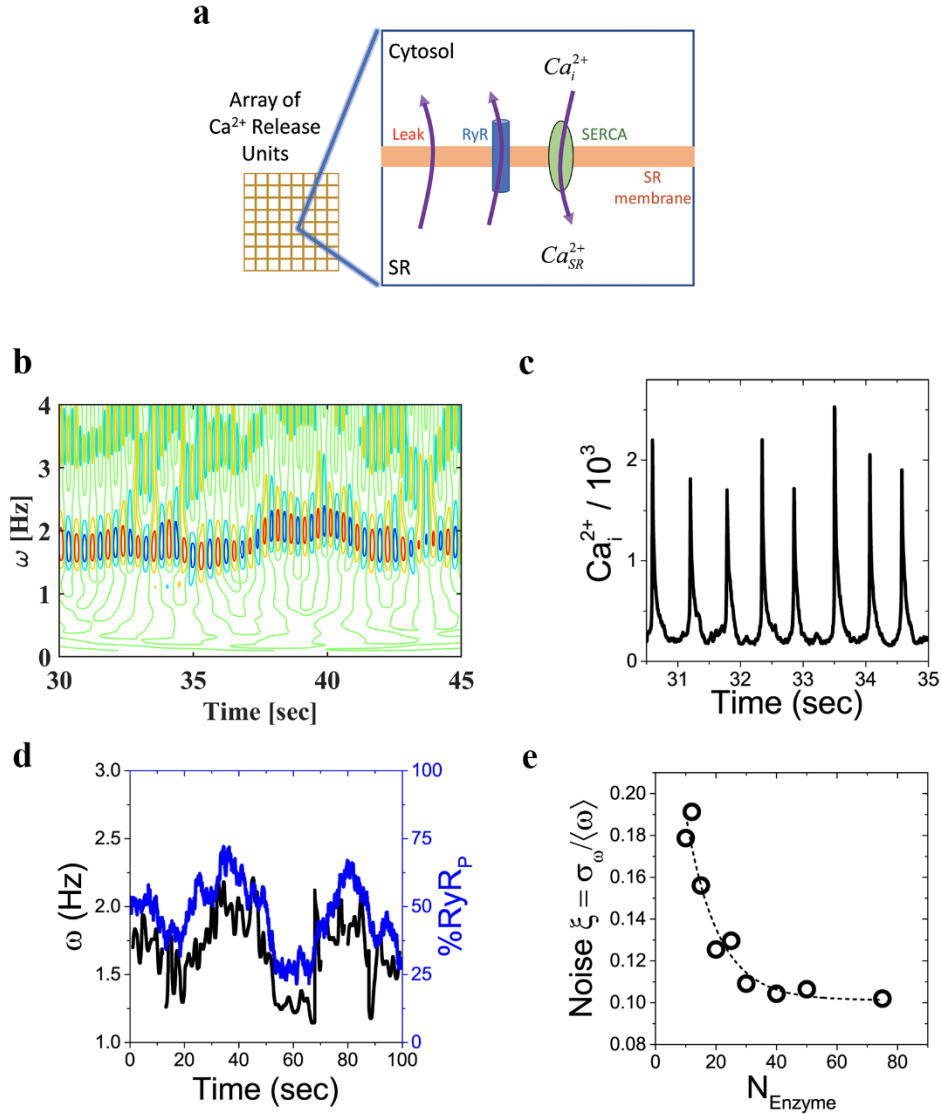


Figure S9: Enzyme-driven noise reduction in a kinetic model for Ca^{2+} oscillations, related to Data S1. a: Schematic illustration of the simplistic kinetic model used to describe Ca^{2+} oscillations in cardiac cells. The model consists of an array of calcium release units (CRUs, the yellow grid), whereby each CRU is divided into two domains, the cytosol and the SR, with local calcium concentrations, Ca_i^{2+} and Ca_{SR}^{2+} , respectively. Calcium can be released from the SR to the cytosol by either leak, or by opening of the *RyR* channels through the CICR mechanism and pumped back to the SR by SERCA. **b-c:** Representative examples for the oscillations of cytosol

calcium concentration, Ca_i^{2+} (b) and for the instantaneous frequency of oscillations vs. time (c) as obtained in the simulation for $N_{\text{Enzyme}} = 50$; $N_{\text{Enzyme}} = N_{\text{kinase}} = N_{\text{phosphatase}}$ is the number of enzymes in the system. The instantaneous frequency was calculated using wavelet analysis of Ca_i^{2+} oscillations. The average frequency is $\sim 1.7\text{Hz}$. **d:** The transient frequency of Ca_i^{2+} oscillations (left, black y-axis) and the transient average percentage of phosphorylated RyR (right, blue y-axis) as a function of time for $N_{\text{Enzyme}} = 10$. The fluctuations in % RyR_P and transient frequency are correlated. **e:** The noise in Ca_i^{2+} frequency decreases as the number of enzymes is increased. The dashed line is a guide to the eye.

	<i>a</i>	<i>k</i>	R²
Fig. 2b (ξ vs. χ for cardiac cells within aligned pairs)	0.46	2.43	0.92
Fig. 2d ($\xi_{\Delta t}$ vs. χ for cardiac cells within aligned pairs)	0.56	2.2	0.96
Fig. 3c (ξ vs. χ for a single cardiac cell interacting with a ‘mechanical cell’)	0.3567	5.11	0.99
Fig. 3d/Fig. 3e (ξ/ξ_0 vs. χ for cardiac cells interacting with a deterministic ‘mechanical cell’)	0.97	5.5	0.95
Fig. 3d (ξ/ξ_0 vs. χ for cardiac cells interacting with a ‘stochastic mechanical cell’)	0.98	2.4	0.97
Fig. 3e (ξ/ξ_0 vs. χ for cardiac cells treated with Colchicine interacting with a deterministic ‘mechanical cell’)	0.98	2	0.96
Fig. 3e (ξ/ξ_0 vs. χ for cardiac cells treated with gp91 interacting with a deterministic ‘mechanical cell’)	0.99	1.14	0.98
Fig. 3e (ξ/ξ_0 vs. χ for cardiac cells treated with AIP interacting with a deterministic ‘mechanical cell’)	1	0.77	0.96

Table S1: Exponential decay fit parameters, related to Figures 2 and 3: Noise (ξ) decays exponentially with the strength of mechanical coupling (χ) according to $\xi = ae^{-k\chi}$. We observe

an exponential decay of beating noise for cells in pairs of mechanically-coupled cardiac cells cultured on a patterned flexible substrate (Fig2) as well as for a single cell interacting with an artificial ‘mechanical cell’ (Fig. 3). Noise is calculated either as the relative standard deviation of the frequency (ξ) or as the relative standard deviation of the time between consecutive contractions ($\xi_{\Delta t}$). ξ_0 is the beating noise prior to probe activation. The coefficients a, k and R-squared for the exponential decays obtained for all these experimental assays are reported in the table above.

Rate constant	Value	Description
$k_{a,NP}$	$1.2 \cdot 10^{24} M^{-4} s^{-1}$	Non-phosphorylated RyR open rate (C1 to O)
$k_{b,NP}$	$18 s^{-1}$	Non-phosphorylated RyR close rate (O to C2)
$k_{c,NP}$	$1.2 s^{-1}$	Non-phosphorylated RyR transition C2 to C1
$k_{a,P}$	$3.6 \cdot 10^{24} M^{-4} s^{-1}$	Phosphorylated RyR open rate (C1 to O)
$k_{b,P}$	$54 s^{-1}$	Phosphorylated RyR close rate (O to C2)
$k_{c,P}$	$3.6 s^{-1}$	Phosphorylated RyR transition C2 to C1
$k_f^{kinase} = k_f^{phosphatase}$	$10^{10} M^{-2} s^{-1}$	Kinase/phosphatase forward rate
$k_r^{kinase} = k_r^{phosphatase}$	$1 s^{-1}$	Kinase/phosphatase reverse rate
$k_{cat}^{kinase} = k_{cat}^{phosphatase}$	$8 s^{-1}$	Kinase/phosphatase catalyst rate constant
k_f^{SERCA}	$3.375 \cdot 10^{15} M^{-2} s^{-1}$	SERCA forward rate
k_r^{SERCA}	$1.1 \cdot 10^4 s^{-1}$	SERCA reverse rate
k_{cat}^{SERCA}	$5.6 \cdot 10^4 s^{-1}$	SERCA catalytic rate (transition of Ca_i^{2+} to Ca_{SR}^{2+})
k_{diff}^{RyR}	$1.7 \cdot 10^7 M^{-1} s^{-1}$	Diffusion rate through RyR^O
k_{diff}^{leak}	$1.5 \cdot 10^7 M^{-1} s^{-1}$	Diffusion rate through SR membrane
$k_{Ca^{2+},diff}^{CRU}$	$5 \cdot 10^3 s^{-1}$	Diffusion of Ca_i^{2+} between neighboring CRUs.
$k_{Enzyme,diff}^{CRU}$	$5 s^{-1}$	Diffusion of kinase/phosphatase between neighboring CRUs.

Table S2. Rate constants used in the kinetic model, related to DataS1

Property		Initial value	Comment
Initial number of molecules per CRU (Total number of CRUs=9)	$RyR_{NP} = RyR_p$	50	
	<i>SERCA</i>	100	
	Ca_i^{2+}	$3 \cdot 10^3$	
	Ca_{SR}^{2+}	$3 \cdot 10^4$	
Volume	Cytosol	$0.525 \mu m^3$	Yields a basal concentration of $Ca_i^{2+} \cong 1 \mu M$
	SR	$0.00525 \mu m^3$	Yields a basal concentration of $Ca_{SR}^{2+} \cong 10mM$

Table S3. SSA simulation parameters, related to DataS1

References

- JONES, E. M. C. 2013. *Improved digital image correlation-*
<http://www.mathworks.com/matlabcentral/fileexchange/43073-improved-digital-image-correlation--dic->
[Online]. Available:
<http://www.mathworks.com/matlabcentral/fileexchange/43073-improved-digital-image-correlation--dic-> [Accessed].
- NITSAN, I., DRORI, S., LEWIS, Y. E., COHEN, S. & TZLIL, S. 2016. Mechanical communication in cardiac cell synchronized beating. *Nat Phys*, 12, 472-477.
- PROSSER, B. L. & WARD, C. W. 2014. Mechano-Chemo Transduction Tunes the Heartstrings. *Science Signaling*, 7, pe7.
- RIBEIRO, A. J. S., ANG, Y.-S., FU, J.-D., RIVAS, R. N., MOHAMED, T. M. A., HIGGS, G. C., SRIVASTAVA, D. & PRUITT, B. L. 2015. Contractility of single cardiomyocytes differentiated from pluripotent stem cells depends on physiological shape and substrate stiffness. *PNAS*, 112, 12705-12710.
- TANG, X., YAKUT ALI, M. & SAIF, M. T. A. 2012. A novel technique for micro-patterning proteins and cells on polyacrylamide gels. *Soft Matter*, 8, 7197-7206.